RHEINISCH-WESTFÄLISCHE TECHNISCHE HOCHSCHULE
AACHEN

MASTER OF SCIENCE THESIS

On the Fokker-Planck Description of the Dense Flows

Author:
Mohsen Sadr

Supervisors:
Dr. M. Hossein Gorji
Prof. Manuel Torrilhon

A thesis submitted in fulfillment of the requirements for the degree of Master of Science

in the

German Research School for Simulation Sciences (GRS)
Mathematics division of the Center for Computational Engineering Science (MathCCES)

January 26, 2017

Declaration of Authorship

I, Mohsen Sadr, declare that this thesis titled, “On the Fokker-Planck Description of the Dense Flows” and the work presented in it are my own. I confirm that:

- This work was done wholly or mainly while in candidature for a research degree at this University.
- Where any part of this thesis has previously been submitted for a degree or any other qualification at this University or any other institution, this has been clearly stated.
- Where I have consulted the published work of others, this is always clearly attributed.
- Where I have quoted from the work of others, the source is always given. With the exception of such quotations, this thesis is entirely my own work.
- I have acknowledged all main sources of help.
- Where the thesis is based on work done by myself jointly with others, I have made clear exactly what was done by others and what I have contributed myself.

Signed:

Date:

"*SOMEWHERE, SOMETHING incredible is waiting to be known.*"

Carl Sagan

On the Fokker-Planck Description of the Dense Flows

Abstract

The classical Navier-Stokes-Fourier system fails to represent the physics of the flow accurately, once a large departure from the equilibrium is concerned. However, main stream methodologies available for computational studies of such flows such as Molecular Dynamics (MD), e.g. see Ullo and Yip, 1984, Direct Simulation Monte-Carlo (DSMC), Bird, 1994, and consistent Boltzmann Algorithm (CBA), Alexander et al., 1995, suffer from quite poor efficiency in particular at high pressure scenarios. The Fokker-Planck model (FP) has been recently introduced by Jenny et al., 2010; Gorji et al., 2011 in order to provide an alternative of DSMC at not too large Knudsen numbers (Kn). It is this property of the FP model which encouraged this project to address the non-equilibrium dense gas flows in a generalized FP framework. In order to cope with that, the Enskog equation is adopted as the governing equation of the dense hard sphere gas. In this thesis, a new advection term is introduced as a reduced order approximation of the Enskog operator. To this end, dense gas effects in the pressure tensor as well as heat fluxes are obtained in accordance with the Enskog expressions. The proposed dense gas FP model is validated in terms of transport properties in comparison with CBA and reference solution.

Acknowledgements

Firstly, I would like to thank Dr. Hossein Gorji for all of his guidance and support during this thesis. I had a great time working with him as I learned new things everyday. He has an unique understanding of kinetic theory and I really appreciate his creative attitude towards research. Therefore, I wish some day I could have the opportunity to do research with him again and learn more about stochastic processes.

Also, my sincere gratitude to Prof. Manuel Torrilhon for making this project possible. While working for him and studying a few courses in his department, the Center for Computational Engineering Science at RWTH Aachen, I was able to expand my knowledge of computational fluid mechanics more fundamentally.

At the end, I would like to thank Information Technology (IT) center of RWTH for providing computational capability that helped me with producing simulation results.

Contents

List of Figures

List of Tables

List of Abbreviations

CBA	**C**onsistent **B**oltzmann **A**lgorithm
DSMC	**D**irect **S**imulation **M**onte **C**arlo
FP	**F**okker **P**lanck
HS	**H**ard **S**phere
IFP	**I**deal gas **F**okker **P**lanck
L-DFP	**L**inear model for **D**ense gas of **F**okker **P**lanck
MD	**M**olecular **D**ynamics
MDF	**M**ass **D**istribution **F**unction
NSF	**N**avier-**S**tokes-**F**ourier
NTC	**N**o **T**ime **C**ounter
Q-DFP	**Q**uadratic model for **D**ense gas of **F**okker **P**lanck

To my parents,
Fatemeh and Bahaeddin

Chapter 1

Introduction

The state of a fluid can be fully determined by knowing the position and the velocity of each constituent particle. Using Newton's law of motion, every state in future can be calculated deterministically. However, since number of particles is typically very large, the corresponding computations become demanding. This is why the classical Molecular Dynamics (MD) is only useful for systems with a few number of particles.

To cope with this problem, the concept of the probability density was utilized in order to describe the state of the fluid. Since typically we are interested only in some macroscopic properties of the fluid flow, the notion of the probability density is sufficient to accurately predict the macroscopic behavior of the flow. This is a very useful concept because, opposed to MD type of approach, here the underlying variable has a solution domain which is independent of the number of particles.

The evolution of the probability distribution function defined over velocity and position can be described by the Boltzmann equation in the case of dilute gases. Yet, due to complexity of the collision integral, Monte-Carlo methods such as Direct Simulation Monte Carlo (DSMC) of Bird, 1994 are typically employed. Similar to the Boltzmann operator, DSMC assumes point particles which provide an ideal gas description. In order to include dense gas effects, Alexander et al., 1995 proposed a simple modification to DSMC, known as Consistent Boltzmann Algorithm (CBA). Since the collision rate in both DSMC and CBA is a function of density, these methods become very expensive as dense gas flows are considered.

In struggle of finding an efficient method with no correlation with respect to the collision rate, the Fokker-Planck (FP) description has been introduced recently by Jenny et al., 2010; Gorji et al., 2011 to describe the Boltzmann operator as an efficient alternative to DSMC. The FP model was developed furthermore for diatomic gases by Gorji and Jenny, 2013. Yet, the available FP model again assumes point particles instead of particles with an actual diameter. The success of the FP model for dilute gas flow simulation together with the fact that the resulting solution algorithm does not employ collision encouraged us to further develop the FP model for dense gases. Therefore, the objective of this thesis is to extend the FP model for dense gases as an efficient alternative of CBA.

There are many applications where an accurate yet efficient mathematical model for the dense gas is highly appreciated. Examples include high pressure shock tubes, cold plasmas, Sonoluminescence, dense nozzle flow, etc. Moreover, this thesis can be considered as a first step to model non-equilibrium liquid phase with a kinetic model.

In this thesis, first in chapter 2 a short review of the kinetic theory is given. Then, Monte-Carlo methods based on Bird's idea, i.e. DSMC and CBA, will be reviewed in chapter 3. In chapter 4, the current FP model of dilute gases will be reviewed. In chapter 5, a new term in the FP model will be proposed which models the dense gas effects in the pressure tensor and the heat fluxes. Some simple simulations are performed and the results are reported in chapter 6 to assess our modeling approach. At the end, conclusion and outlooks for further studies are given in chapter 7.

Chapter 2

Kinetic Theory

Instead of field quantities concerned in the continuum fluid mechanics, the kinetic theory focuses on the distribution functions in the whole phase space. The probability density function (PDF) $f(\boldsymbol{V}, \boldsymbol{x}, t)$ is defined such that $f(\boldsymbol{V}, \boldsymbol{x}, t)d^3\boldsymbol{V}$ gives the probability of finding a particle inside the infinitesimal volume $d^3\boldsymbol{V}$ around $\boldsymbol{V}$ at the position $\boldsymbol{x}$ and time t. Usually the mass density function (MDF) is used in the kinetic theory

$$\mathcal{F}(\boldsymbol{V}, \boldsymbol{x}, t) = \rho(\boldsymbol{x}, t) f(\boldsymbol{V}, \boldsymbol{x}, t), \tag{2.1}$$

where ρ is density of gas. By integrating MDF over the velocity space, we obtain the density

$$\rho(\boldsymbol{x}, t) = \int_{R^3} \mathcal{F} d^3\boldsymbol{V}^{1}. \tag{2.2}$$

The expected value of a quantity $\phi(\boldsymbol{V})$ can be found based on the MDF

$$\langle \psi(\boldsymbol{M}) \rangle = \frac{1}{\rho} \int_{R^3} \phi(\boldsymbol{V}) \mathcal{F} d^3\boldsymbol{V}, \tag{2.3}$$

where $\boldsymbol{M}(t)$ is a random variable from the space $\boldsymbol{V}$. Macroscopic properties can be also obtained from MDF. The bulk velocity is nothing but mean velocity of particles, i.e. for $i \in \{1, 2, 3\}$ being index of velocity domain

$$\begin{aligned} U_i &= \frac{1}{\rho} \int_{R^3} \mathcal{F} V_i d^3\boldsymbol{V} \\ &= \langle M_i \rangle. \end{aligned} \tag{2.4}$$

The temperature in the kinetic theory is defined in terms of the fluctuating velocity, i.e.

[1] $d^3\boldsymbol{V}$ is short for $dV_1 dV_2 dV_3$

$$T = \frac{1}{3nk_b}\int_{R^3} \mathcal{F} v'_j v'_j d^3\boldsymbol{V} \tag{2.5}$$

$$= \frac{m}{3k_b}\langle M'_j M'_j\rangle, \tag{2.6}$$

with m the particle mass, k_b the Boltzmann constant, $v'_i = V_i - U_i$ and n the number density. Note that the Einstein notation is used everywhere in this thesis unless it is mentioned otherwise.

Furthermore, the shear stress and the heat fluxes are closed once the MDF is known. The pressure tensor is calculated by taking second moment $v'_i v'_j$ of the MDF

$$\pi_{ij} = \int_{R^3} \mathcal{F} v'_i v'_j d^3\boldsymbol{V}$$

$$= \rho\langle M'_i M'_j\rangle. \tag{2.7}$$

Like any other tensor, the pressure tensor can be decomposed into two parts: trace and deviatoric part. The trace gives the pressure while the deviotoric part leads to the shear stress

$$\tau_{ij} = -\pi_{\langle ij\rangle}$$

$$= -\rho\langle M'_{\langle i} M'_{j\rangle}\rangle, \tag{2.8}$$

$$P = \pi_{ii}/3$$

$$= \rho\langle M'_i M'_i\rangle/3, \tag{2.9}$$

where $\boldsymbol{\tau}$ indicates the shear stress and P the pressure. Therefore

$$\pi_{ij} = -\tau_{ij} + \delta_{ij}P \quad \text{and} \tag{2.10}$$

$$\rho\langle M'_i M'_j\rangle = \rho\langle M'_{\langle i} M'_{j\rangle}\rangle + \rho\langle M'_k M'_k\rangle\delta_{ij}/3. \tag{2.11}$$

Bra and ket in the subscript represent the deviatoric part of the tensor. By taking the third moment $v'_i v'_j v'_j$ of the MDF, we get the heat flux vector

$$q_i = \frac{1}{2}\int_{R^3} \mathcal{F} v'_i v'_j v'_j d^3\boldsymbol{V}$$

$$= \frac{1}{2}\rho\langle M'_i M'_j M'_j\rangle. \tag{2.12}$$

As it was mentioned before, in many situations the gas may exhibit non-continuum behaviors, such that the macroscopic quantities do not form a closed set of PDEs, but depend on microscopic collisions. This scenario which happens e.g. in shocks or micro/nano systems can be characterized by the Knudsen number

$$Kn = \frac{\lambda}{L}, \tag{2.13}$$

where λ indicates the mean free path and L is a macroscopic length scale of the problem under consideration. The mean free path is simply the average distance that particles travel between successive collisions. For hard sphere gas at the equilibrium one can show that

$$\lambda = \frac{1}{\sqrt{2} n \pi \sigma^2}, \tag{2.14}$$

where σ is the molecular diameter, see Bird, 1994.

2.1 Evolution of MDF

The evolution of a single particle distribution $\mathcal{F}(\boldsymbol{V}, \boldsymbol{x}, t)$ in gas may be expressed in a generic form

$$\frac{\partial \mathcal{F}}{\partial t} + \frac{\partial (\mathcal{F} V_i)}{\partial x_i} + \frac{\partial (\mathcal{F} G_i)}{\partial V_i} = S_{coll}(\mathcal{F}), \tag{2.15}$$

where S_{coll} is the collision operator accounting for the binary collisions among molecules and $\boldsymbol{G}$ represents external force per mass. Considering dilute gas and molecular chaos assumptions one can derive the Boltzmann operator while by including the diameter of particle the Enskog operator can be obtained.

It is important to note that any collision operator for a monatomic gas must conserve mass, momentum and energy. In other words, for any $\Psi_{cons} \in \{1, V_i, V_j V_j\}$ the following condition must hold

$$\int_{R^3} \Psi_{cons} S_{coll}(\mathcal{F}) d^3\boldsymbol{V} = 0 \quad \text{for any} \quad \mathcal{F}. \tag{2.16}$$

Moreover, considering a homogeneous setting, i.e. $\mathcal{F}(\boldsymbol{V}, t)$ the equilibrium is a Maxwellian distribution

$$\mathcal{F}_M = \frac{\rho}{(2\pi k_b T/m)^{3/2}} exp\Big[- \frac{(V_i - U_i)(V_i - U_i)}{2 k_b T/m} \Big] \quad \text{and} \tag{2.17}$$

$$S(\mathcal{F}) = 0 \rightarrow \mathcal{F} = \mathcal{F}_M. \tag{2.18}$$

Therefore, any description for $S_{coll}(\mathcal{F})$ must satisfy these two conditions, i.e. eq. (2.16) and eq. (2.18), to be a valid model from physical principles. Also, in order to obtain identical transport properties for any $S^{model}(\mathcal{F})$ compared to a true collision operator $S_{coll}(\mathcal{F})$, their first few moments should match

$$\int_{R^3} \Psi S^{model}(\mathcal{F}) d^3\boldsymbol{V} = \int_{R^3} \Psi S_{coll}(\mathcal{F}) d^3\boldsymbol{V}, \tag{2.19}$$

where $\Psi = \{V_i V_j, V_i V_j V_k, ..., V_{i_1} ... V_{i_M}\}$. This condition will be used for obtaining drift and diffusion coefficients of the Fokker Planck description in chapter 4. By taking moments $\Phi = \{v'_{\langle i} v'_{j\rangle}, v'_i v'_j v'_j\}$ of homogeneous transport equation, one can show that the relaxation rate of shear the stress and heat fluxes are

$$\frac{\partial \pi_{ij}}{\partial t} = \int_{R^3} v'_{\langle i} v'_{j\rangle} S_{coll} d^3\boldsymbol{V} \quad \text{and} \tag{2.20}$$

$$\frac{\partial q_i}{\partial t} = \frac{1}{2} \int_{R^3} v'_i v'_j v'_j S_{coll} d^3\boldsymbol{V}. \tag{2.21}$$

2.2 Boltzmann Operator

By adopting two main assumptions, the Boltzmann equation describes the evolution of $\mathcal{F}$ with S^{Boltz} being the collision operator.

The first assumption is the dilute gas model. Accordingly, the molecules are considered to be point particles. Therefore, the MDF of colliding particles are at the same point in space. This simplifies the collision integral and is valid when the gas is dilute enough. Meaning that the average distance between particles is significantly larger than molecular diameter.

The second assumption is the principle of *molecular chaos*. A binary collision involves the distribution of two particles in the phase space, namely $\mathcal{F}(\boldsymbol{V}_1, \boldsymbol{V}_2, \boldsymbol{x}_1, \boldsymbol{x}_2, t)$. The molecular chaos assumption is simply that $\mathcal{F}(\boldsymbol{V}_1, \boldsymbol{V}_2, \boldsymbol{x}_1, \boldsymbol{x}_2, t) = \mathcal{F}(\boldsymbol{V}_1, \boldsymbol{x}_1, t)\mathcal{F}(\boldsymbol{V}_2, \boldsymbol{x}_2, t)$.

Hence, Boltzmann operator can be derived for S_{coll}

$$S^{Boltz} = \int_{R^3} \int_0^{2\pi} \int_0^{+\infty} \Big(\mathcal{F}(\boldsymbol{V}^*, \boldsymbol{x})\mathcal{F}(\boldsymbol{V}_1^*, \boldsymbol{x}) - \mathcal{F}(\boldsymbol{V}, \boldsymbol{x})\mathcal{F}(\boldsymbol{V}_1, \boldsymbol{x})\Big) g \hat{b} d\hat{b} d\hat{\epsilon} d^3\boldsymbol{V}, \tag{2.22}$$

where $\boldsymbol{V}$ and $\boldsymbol{V}_1$ are velocities of the colliding couple before collision whereas $\boldsymbol{V}^*$ and $\boldsymbol{V}_1^*$ represent the corresponding post-collision velocities. Here, g is the magnitude of relative velocity $g = |\boldsymbol{V} - \boldsymbol{V_1}|$. $\hat{b}$ and $\hat{\epsilon}$ are collision parameter and collision angle $\hat{\epsilon} \in [0, 2\pi]$, respectively. For derivation and details of the collision integral, see e.g. Chapman and Cowling, 1953.

One can obtain relaxation rates of different velocity moments based on S^{Boltz} by taking moments of $S^{boltz}(\mathcal{F})$, e.g.

$$P_{ij} = \int_{R^3} v'_{\langle i} v'_{j\rangle} S^{Boltz} d^3\boldsymbol{V} \quad \text{and} \tag{2.23}$$

$$P_i = \int_{R^3} v'_i v'_j v'_j S^{Boltz} d^3\boldsymbol{V}. \tag{2.24}$$

Assuming Maxwell molecules and substituting P_{ij} and P_i in eqs. (2.20) and (2.21) one can get

$$\frac{\partial \pi_{ij}}{\partial t} = -\frac{P}{\mu}\pi_{ij} \quad \text{and} \tag{2.25}$$

$$\frac{\partial q_i}{\partial t} = -\frac{2}{3}\frac{P}{\mu}q_i, \tag{2.26}$$

where μ is the viscosity in the Chapman-Enskog limit, see Cercignani, 1988. Therefore, the Boltzmann collision operator correctly predicts the viscosity and the Prandtl number at the hydrodynamic limit. In monatomic gases at the hydrodynamic limit $Pr = 2/3$, see Truesdell and Muncaster, 1980, which is consistent with S^{Boltz}.

2.2.1 Moments of the Boltzmann Equation

Multiplying both sides of the Boltzmann equation with $\psi \in \{1, V_i, V_iV_i\}$ and taking integral over the velocity space, one can get the continuity, mass and energy conservations. In the derivations one should use the fact that the MDF vanishes as $\boldsymbol{V} \to \pm\infty$. More precisely, we get

$$\frac{\partial \rho}{\partial t} + \frac{\partial(\rho U_\alpha)}{\partial x_\alpha} = 0, \tag{2.27}$$

$$\frac{\partial(\rho U_\alpha)}{\partial t} + \frac{\partial(\rho U_\alpha U_\beta)}{\partial x_\beta} + \frac{\partial \pi_{\alpha\beta}}{x_\beta} = 0; \quad \alpha = 1,2,3 \quad \text{and} \tag{2.28}$$

$$\frac{\partial E}{\partial t} + \frac{\partial(EU_\beta)}{\partial x_\beta} + \frac{\partial \pi_{\alpha\beta}U_\beta}{x_\alpha} + \frac{\partial q_\beta}{\partial x_\beta} = 0. \tag{2.29}$$

Equations (2.27) to (2.29) represent balance laws when macroscopic quantities are defined as moments of the distribution. Here, E is the total energy, i.e. $E = c_v T + \rho U_i U_i/2$ where c_v is the heat capacity in constant volume i.e. $c_v = 3k_b/(2m)$ for monatomic gas.

2.2.2 Navier-Stokes-Fourier System of Equations

Provided that the MDF is only slightly perturbed from the Maxwellian distribution, it is useful to consider the expansion $\mathcal{F} = \mathcal{F}^{(0)} + e\mathcal{F}^{(1)} + ...$ where $e = Kn$. By inserting the asymptotic expansion in the Boltzmann equation and keeping the first order terms, the Navier-Stokes-Fourier (NSF) system is obtained. This procedure

is called the Chapmann-Enskog expansion which provides closure equations for pressure tensor and heat fluxes, see Chapman and Cowling, 1953.

The above-mentioned closures for the NSF limit then take the form

$$\tau_{ij} = \mu(\frac{\partial U_i}{\partial x_j} + \frac{\partial U_j}{\partial x_i}) - \frac{2\mu}{3}\delta_{\alpha\beta}\frac{\partial U_\gamma}{\partial x_\gamma} \quad \text{and} \tag{2.30}$$

$$q_i = -\kappa\frac{\partial T}{\partial x_i}. \tag{2.31}$$

Here, κ represents the coefficient of heat conductivity.

2.3 Enskog Operator

Obviously as the number density or the molecular diameter increases, the underlying dilute gas assumption breaks down and hence a more accurate S_{coll} compared to S^{Boltz} should be adopted. Enskog has modified the Boltzmann equation in order to deal with this so-called dense gas effect. First modification was including the distance of colliding particles in their MDF. It becomes simply the molecular diameter σ in case of the hard sphere model.

Next, the collision rate increases by the factor Y due to the correlation between the collision pair. The idea is that volume occupied by the molecules becomes comparable with the whole volume of the gas. Therefore, there will be more collisions compared to the dilute limit. Y equals to unity in case of rarefied gas and goes to infinity when the particles becomes so close to each other that they cannot move anymore. Note that Y is a function of density and increases with it. Assuming small nb factor, Boltzmann and Clausius proposed the following expression for Y

$$Y = 1 + 0.625nb + 0.2869(nb)^2 + 0.115(nb)^3, \tag{2.32}$$

where $b = \frac{2}{3}\pi\sigma^3$ is called the HS second virial coefficient, see Chapman and Cowling, 1953. Based on the above-mentioned modifications Enskog proposed a modified collision operator including dense gas effects

$$S_{coll} \approx S^{Enskog} = \int_{R^3}\int_0^{2\pi}\int_0^{+\infty}\Big[Y(\boldsymbol{x} + \frac{1}{2}\sigma\hat{\boldsymbol{k}})\mathcal{F}(\boldsymbol{V}^*, \boldsymbol{x})\mathcal{F}(\boldsymbol{V}_1^*, \boldsymbol{x}_1 + \sigma\hat{\boldsymbol{k}}) - Y(\boldsymbol{x} - \frac{1}{2}\sigma\hat{\boldsymbol{k}})\mathcal{F}(\boldsymbol{V}, \boldsymbol{x})\mathcal{F}(\boldsymbol{V}_1, \boldsymbol{x}_1 - \sigma\hat{\boldsymbol{k}})\Big]g\hat{b}d\hat{b}d\hat{\epsilon}d^3\boldsymbol{V}. \tag{2.33}$$

Note that $\hat{\boldsymbol{k}}$ is the normal vector connecting centers of two colliding hard spheres, $\hat{\boldsymbol{k}} = (\boldsymbol{x} - \boldsymbol{x}_1)/\|\boldsymbol{x} - \boldsymbol{x}_1\|_2$. For more details of the Enskog collision operator reader is referred to Chapman and Cowling, 1953; Hirschfelder et al., 1963. By Taylor expansion of $Y(\boldsymbol{x} + \frac{1}{2}\sigma\hat{\boldsymbol{k}})$, $\mathcal{F}(\boldsymbol{V}_1^*, \boldsymbol{x}_1 + \sigma\hat{\boldsymbol{k}})$ and $\mathcal{F}(\boldsymbol{V}_1, \boldsymbol{x}_1 - \sigma\hat{\boldsymbol{k}})$ one can show that

$$S^{Enskog} = Y(\boldsymbol{x})S^{Boltz} + S_\phi, \tag{2.34}$$

where S_ϕ stands for the collision contributions due to the molecular potential. S_ϕ is an infinite sum of integrals

$$S_\phi = J_1 + J_2 + J_3 + J_4 + J_5 + J_6 + \dots . \tag{2.35}$$

Following expressions can be found for J_1 to J_6

$$J_1 = Y \int_{R^3} \int_0^{2\pi} \int_0^{+\infty} (\mathcal{F}^* \mathcal{F}_1^* - \mathcal{F}\mathcal{F}_1) g \hat{b} d\hat{b} d\hat{\epsilon} d^3\boldsymbol{V}, \tag{2.36}$$

$$J_2 = \sigma Y \int_{R^3} \int_0^{2\pi} \int_0^{+\infty} \Big(k_i (\mathcal{F}^* \frac{\partial \mathcal{F}_1^*}{\partial x_i} + \mathcal{F} \frac{\partial \mathcal{F}_1}{\partial x_i})\Big) g \hat{b} d\hat{b} d\hat{\epsilon} d^3\boldsymbol{V}, \tag{2.37}$$

$$J_3 = \frac{\sigma}{2} \int_{R^3} \int_0^{2\pi} \int_0^{+\infty} (k_i \frac{\partial Y}{\partial x_i})(\mathcal{F}^* \mathcal{F}_1^* - \mathcal{F}\mathcal{F}_1) g \hat{b} d\hat{b} d\hat{\epsilon} d^3\boldsymbol{V}, \tag{2.38}$$

$$J_4 = \frac{\sigma^2}{2} Y \int_{R^3} \int_0^{2\pi} \int_0^{+\infty} \Big(k_i k_j (\mathcal{F}^* \frac{\partial^2 \mathcal{F}_1^*}{\partial x_i \partial x_j} - \mathcal{F} \frac{\partial^2 \mathcal{F}_1}{\partial x_i \partial x_j})\Big) g \hat{b} d\hat{b} d\hat{\epsilon} d^3\boldsymbol{V}, \tag{2.39}$$

$$J_5 = \frac{\sigma^2}{2} \int_{R^3} \int_0^{2\pi} \int_0^{+\infty} (k_i \frac{\partial Y}{\partial x_i})\Big(k_j (\mathcal{F}^* \frac{\partial \mathcal{F}_1^*}{\partial x_j} - \mathcal{F} \frac{\partial \mathcal{F}_1}{\partial x_j})\Big) g \hat{b} d\hat{b} d\hat{\epsilon} d^3\boldsymbol{V} \quad \text{and} \tag{2.40}$$

$$J_6 = \frac{\sigma^2}{8} \int_{R^3} \int_0^{2\pi} \int_0^{+\infty} (k_i k_j \frac{\partial^2 Y}{\partial x_i \partial x_j})(\mathcal{F}^* \mathcal{F}_1^* - \mathcal{F}\mathcal{F}_1) g \hat{b} d\hat{b} d\hat{\epsilon} d^3\boldsymbol{V}. \tag{2.41}$$

For details see Hirschfelder et al., 1963. Since S_ϕ equals to zero in the homogeneous setup, similar to eqs. (2.25) and (2.26), one can show that the relaxation rates of the shear stress and the heat fluxes are

$$\frac{\partial \pi_{ij}}{\partial t} = -Y \frac{p}{\mu} \pi_{ij} \quad \text{and} \tag{2.42}$$

$$\frac{\partial q_i}{\partial t} = -Y \frac{2}{3} \frac{p}{\mu} q_i, \tag{2.43}$$

respectively.

2.3.1 Collisional Transfer of Molecular Quantities

Taking moments of the Enskog equation may not lead to explicit expressions. By transferring the physical coordinate to $\boldsymbol{x} - \boldsymbol{r}$ with $\boldsymbol{r}$ being the contact point of colliding particles, total rate of collision transport of $\psi(\boldsymbol{V})$ across $d\boldsymbol{S}$ per unit of time and area becomes

$$\sigma Y(\boldsymbol{r}) \int_{R^3}\int_{R^3}\int_0^{2\pi}\int_0^{+\infty} (\psi' - \psi)\mathcal{F}(\boldsymbol{V}, \boldsymbol{r} + \frac{\sigma}{2}\hat{\boldsymbol{k}})\mathcal{F}(\boldsymbol{V}_1, \boldsymbol{r}_1 + \frac{\sigma}{2}\hat{\boldsymbol{k}})(\hat{\boldsymbol{k}}.\boldsymbol{n})g\hat{b}d\hat{b}d\hat{\epsilon}d^3\boldsymbol{V}d^3\boldsymbol{V}_1, \tag{2.44}$$

where $\boldsymbol{n}$ is normal of $d\boldsymbol{S}$. Again, using Taylor expansion and ignoring derivatives of second and higher orders, the collision part of the vector of flow of ψ can be simplified to

$$\begin{aligned}&\frac{1}{2}\sigma Y(\boldsymbol{r}) \int_{R^3}\int_{R^3}\int_0^{2\pi}\int_0^{+\infty} (\psi' - \psi)\mathcal{F}\mathcal{F}_1\hat{\boldsymbol{k}}g\hat{b}d\hat{b}d\hat{\epsilon}d^3\boldsymbol{V}d^3\boldsymbol{V}_1 \\ &+ \frac{1}{4}\sigma^2 Y(\boldsymbol{r}) \int_{R^3}\int_{R^3}\int_0^{2\pi}\int_0^{+\infty} (\psi' - \psi)\mathcal{F}\mathcal{F}_1\hat{k}_j.\frac{\partial}{\partial r_j}(log(\mathcal{F}/\mathcal{F}_1)\hat{\boldsymbol{k}}g\hat{b}d\hat{b}d\hat{\epsilon}d^3\boldsymbol{V}d^3\boldsymbol{V}_1,\end{aligned} \tag{2.45}$$

see Hirschfelder et al., 1963. Chapman and Cowling, 1953 showed that for $\psi \in \{V_i, V_jV_j\}$, collisional transfers of momentum and energy lead to

$$\begin{aligned}\pi_{ij} &= \Big(nkT(1 + nbY) - w\frac{\partial U_k}{\partial x_k}\Big)\delta_{ij} \\ &\quad + \rho(1 + 2nbY/5)\langle M'_{\langle i}M'_{j\rangle}\rangle - (5w/6)\frac{\partial U_{\langle i}}{\partial x_{j\rangle}} \quad \text{and} \qquad (2.46)\\ q_i &= \frac{1}{2}\rho(1 + 3nbY/5)\langle M'_iM'_jM'_j\rangle - c_v w\frac{\partial T}{\partial x_i}, \qquad (2.47)\end{aligned}$$

where $c_v = 3k/(2m)$ and

$$\begin{aligned}w &= (nb)^2 Y\sqrt{mk_bT}/(\pi^{3/2}\sigma^2) \\ &= 1.002\mu Y(nb)^2.\end{aligned} \tag{2.48}$$

Here μ is the HS viscosity in the dilute limit

$$\mu = 1.016 \times 5\sqrt{mk_bT}/(16\sqrt{\pi}\sigma^2). \tag{2.49}$$

Using the Chapmann-Enskog expansion one can provide first and second approximations to $\langle M'_iM'_j\rangle$ and $\langle M'_iM'_jM'_j\rangle$ as discussed in the following.

2.3.2 Chapman-Enskog Expansion of the Enksog Equation

Expressions (2.46) and (2.47) can be further simplified by using Chapman-Enskog expansion for the unclosed terms $\langle M'_iM'_j\rangle$ and $\langle M'_iM'_jM'_j\rangle$. Following the same methodology as in the dilute gas case, i.e. $\mathcal{F} \approx \mathcal{F}^{(0)} + Kn\mathcal{F}^{(1)}$, the NSF closures of the dense gas becomes (Chapman and Cowling, 1953)

$$\pi_{ij} = \Big(nkT(1+nbY) - w\frac{\partial U_k}{\partial x_k}\Big)\delta_{ij} - \Big(\frac{2\mu^k}{Y}(1+2nbY/5)^2 + 5w/6\Big)\frac{\partial U_{\langle i}}{\partial x_{j\rangle}}, \quad \text{and} \tag{2.50}$$

$$q_i = -\Big(\frac{1}{Y}(1+3nbY/5)^2\kappa^k + c_v w\Big)\frac{\partial T}{\partial x_i}, \tag{2.51}$$

with μ^k and κ^k the viscosity and the heat conductivity of dilute gas limit.

Chapter 3

Review of Bird's Algorithm

Since direct simulations based on the Boltzmann equation impose formidable challenges due to the high dimensionality of the phase space, several attempts have been made in order to provide an alternative solution algorithm. In 60's, Bird, 1963 proposed a Monte-Carlo algorithm in order to simulate rarefied gas flows consistent with the Boltzmann equation. Direct Simulation Monte Carlo (DSMC) therefore was introduced by Bird, 1994, where later it has been proven to be consistent with the Boltzmann equation. The idea is to employ computational particles as discretization of the MDF. Same limitations which exist in the Boltzmann equation are also implied in DSMC, i.e. dilute gas and molecular chaos. Therefore, DSMC is not accurate once applied directly for simulating dense gases. Alexander et al., 1995 provided a modification to DSMC such that dense effects could be captured. Their so-called Consistent Boltzmann Algorithm (CBA) employs correction in the position of the particles to mimic the dense gas effects. In this chapter, algorithms of DSMC and CBA will be explained and their pros and cons will be discussed.

3.1 DSMC Algorithm

In DSMC, computational particles are employed whose positions and velocities are updated in two steps: streaming and collision. The former is simply the direct flight of particle. The latter involves selecting the collision candidates and consequently performing collisions. Since collisions happen among nearby particles, a discretization of the physical space is necessary as well. Therefore, particles only interact inside each cell.

Let Λ_{coll} be the number of candidate pairs for collision. Λ_{coll} out of N_c, i.e. number of computational particles inside the cell c, are selected according to No Time Counter (NTC) method, eq. (3.1). Λ_{coll} is itself a function of upper bound value

$$\Lambda_{max} = F_N N_C^2 \pi \sigma^2 M_{r,max} \Delta t / V_c, \tag{3.1}$$

where $M_{r,max}$ is the magnitude of a maximum relative velocity of any pair within the cell, V_c the volume of the cell and F_N the number of physical particles that each computational particle represents. Whether the picked pair actually collide or not depends on the condition which for HS gas becomes

$$M_r / M_{r,max} > r, \tag{3.2}$$

1.	Stream particles with their current velocity.
2.	Apply boundary conditions.
3.	Update velocity according to collisions.
4.	Sample data.

TABLE 3.1: Outline of the DSMC algorithm for each time step.

with M_r the magnitude of the relative velocity of the selected pair and r is a random number between zero and one with the uniform distribution.

Once eq. (3.2) is satisfied, the velocities of the selected pair are updated. Conservation of the linear momentum requires the the velocity of the center of mass remains unchanged while energy conservation implies that the magnitude of the relative velocity stays constant during the collision. Therefore, there is still freedom with respect to directions to which particles scatter. According to the HS model, the relative velocity vector should scatter isotropically. Therefore, the following updates

$$\boldsymbol{M}_r^{post} = M_r^{post}(cos\theta, sin\theta cos\phi, sin\theta sin\phi)^T, \tag{3.3}$$

$$\phi = 2\pi\alpha_1 \quad \text{and} \tag{3.4}$$

$$cos\theta = 1 - 2\alpha_2, \tag{3.5}$$

with α_1 and α_2 being uniform random numbers between zero and one, are adopted. For more details on DSMC see Bird, 1994. Here, an outline of the DSMC algorithm is given in table 3.1.

3.2 CBA Algorithm

As mentioned in the begining of this chapter, DSMC similar to the Boltzmann operator assumes point particles instead of particles with a physical diameter. This assumption is only valid when gas is dilute enough. To cope with that in dense gases, Alexander et al., 1995 suggested a simple modification to DSMC such that dense effects can be captured within the DSMC framework. Two modifications are introduced in CBA accordingly. First, a position correction upon colliding particles due to their diameter. Second, an extra collision due to the pair correlation function Y (see eq. (2.32)).

Therefore, after each collisions the two colliding particles are transported with an extra factor of $\pm\boldsymbol{d}$, where

$$\boldsymbol{d} = \frac{\boldsymbol{M}_r^* - \boldsymbol{M}_r}{||\boldsymbol{M}_r^* - \boldsymbol{M}_r||_2}\sigma \tag{3.6}$$

and $*$ denotes the post-collision value. Hence, one particle is streamed $+\boldsymbol{d}$ and the other $-\boldsymbol{d}$ in addition to their normal streaming. Furthermore, the number of collisions is modified such that,

$$\Lambda_{coll}^{CBA} = Y\Lambda_{coll}^{Boltz}. \tag{3.7}$$

1.	Stream particles with their current velocities.
2.	Apply boundary conditions.
3.	**Update velocity and position according to dense gas collisions**.
4.	**Apply boundary conditions**.
5.	Sample data.

TABLE 3.2: Outline of the CBA algorithm for each time step.

An outline of the CBA algorithm is given in table 3.2. In comparison to DSMC, step three is modified and step four is added. The reason is that in the velocity update, i.e. step 3, positions are also updated. Thus, boundary conditions need to be checked again after collisions. Alexander et al., 1995 showed that their approach predicts transport coefficients of dense gases for a considerable density range. Yet, once $n\sigma > 0.4$ CBA diverges from MD and Enskog's solution.

The main drawback in the CBA algorithm is the fact that Λ_{coll}^{CBA} becomes quite large for dense gases. Since so many collisions have to be performed in each time step, which increase quadratically with the number density, CBA is not employed often in dense gas simulations. This is one of the motivations for expanding the Fokker-Planck model for dense gases, since its complexity has no direct correlation with the number density of the fluid.

Chapter 4

Fokker-Planck Kinetics

In this chapter, a short review of the Fokker-Planck approximation of the Boltzmann collision operator will be given and the recent developments will be discussed. Please note that in this chapter still particles are assumed to be point particles with no diameter. In chapter 5, a more relative model for dense gases will be proposed.

4.1 The Fokker-Planck Equation

The Fokker-Planck kinetic equation can be regarded as an approximation of the Boltzmann equation in a sense that here we replace a jump process with a continuous one. The idea is to describe the evolution of the MDF by two contributing forces: drift and diffusion.

Suppose $\boldsymbol{M}$ denotes random variable from the velocity space $\boldsymbol{V}$ and $\boldsymbol{X}$ random variable from $\boldsymbol{x}$. For a process described by the following stochastic differential equations (SDEs)

$$d\boldsymbol{p} = \widetilde{\boldsymbol{A}}dt + \boldsymbol{\lambda}d\boldsymbol{W} \tag{4.1}$$

where $\boldsymbol{W}$ is a Wiener process,

$$\boldsymbol{p} = \begin{pmatrix} M_1 \\ M_2 \\ M_3 \\ X_1 \\ X_2 \\ X_3 \end{pmatrix}, \qquad \boldsymbol{\lambda} = \begin{pmatrix} D_{11} & D_{12} & D_{13} & 0 & 0 & 0 \\ D_{21} & D_{22} & D_{23} & 0 & 0 & 0 \\ D_{31} & D_{32} & D_{33} & 0 & 0 & 0 \\ 0 & 0 & 0 & 0 & 0 & 0 \\ 0 & 0 & 0 & 0 & 0 & 0 \\ 0 & 0 & 0 & 0 & 0 & 0 \end{pmatrix} \text{ and } \qquad \widetilde{\boldsymbol{A}} = \begin{pmatrix} A_1 \\ A_2 \\ A_3 \\ M_1 \\ M_2 \\ M_3 \end{pmatrix}, \tag{4.2}$$

the Itô calculus provides us the equivalent Fokker-Planck equation

$$\frac{\partial \mathcal{F}}{\partial t} + \frac{\partial (\mathcal{F} V_i)}{\partial x_i} = -\frac{\partial (\mathcal{F} A_i)}{\partial V_i} + \frac{1}{2}\frac{\partial^2}{\partial V_i \partial V_j}(D_{ik} D_{kj} \mathcal{F}), \tag{4.3}$$

where $i, j \in \{1, 2, 3\}$. The coefficients A_i and D_{ij} are called drift and diffusion coefficients, respectively. For details of this link, reader is referred to Gardiner, 1996. Let us call the right hand side of eq. (4.3) S^{FP}. This operator, like any other operator that approximates collision integral, naturally must satisfy conservations i.e.

eq. (2.16) and the equilibrium conditions i.e. eqs. (2.17) and (2.18). In the first attempt in literature, first a linear model for A_i and a scalar D were proposed (known as linear FP) by Jenny et al., 2010. Also it was shown that their linear model provides a wrong value for the Prandtl number of monatomic gas in the hydrodynamic limit. Then, Gorji et al., 2011 fixed this problem by providing a cubic model for the drift. Since the cubic model with vanishing cubic term still provides a correct Prandtl number, in this study for simplicity we focus on the quadratic version of the cubic model. Note that once high Mach flows are considered, the cubic term should be taken into account for stability reasons.

4.2 Linear Drift Model

Jenny et al., 2010 proposed a linear drift model for the Fokker-Planck description of the Boltzmann operator which satisfies the conservation of mass, momentum and energy besides H-theorem. This linear drift model can be constructed such that the evolution of moments become consistent with the Boltzmann equation up to the shear stresses. Therefore, the following closures were considered

$$A_i = -\frac{1}{\tau} v_i', \tag{4.4}$$

$$D_{ij} = \sqrt{\frac{2kT}{\tau m}} \delta_{ij} \quad \text{and} \tag{4.5}$$

$$\tau = 2\mu/P. \tag{4.6}$$

However, this closure gives rise to a wrong Prandtl number of $3/2$, instead of its correct value for the monatomic gas.

4.3 Quadratic Drift Model

Gorji et al., 2011 developed FP model of monatomic gas such that in the hydrodynamic limit the correct Prandtl number can be achieved. More accurately, for non-equilibrium relaxation rates of the shear stress and heat fluxes the model must provide specific rates, i.e. eq. (2.25) and eq. (2.26) respectively. Due to stability reasons, they considered a cubic ansatz for the drift, even though a quadratic one suffices to fix the correct Prandtl number. Therefore, in this study for simplicity we consider the cubic model with the vanishing cubic term.

The idea is to provide closures for A_i and D_{ik} such that same transport properties corresponding to the Boltzmann equation are obtained. In other words, the moments of S^{FP} must be equal to the moments of the Boltzmann collision integral. As discussed in chapter 2, this constraint on FP will provide eventually similar relaxation rates for the shear stress eq. (2.25) and the heat fluxes eq. (2.26). To satisfy these constraints, it would be enough to consider a quadratic model for A_i and a scalar for D_{ij}, i.e.

$$A_i = -\frac{1}{\tau}v_i' + c_{ij}v_j' + \gamma_i(v_j'v_j' - \frac{3kT}{m}), \tag{4.7}$$

$$D_{ij} = \sqrt{\frac{2kT}{\tau m}}\delta_{ij} \quad \text{and} \tag{4.8}$$

$$\tau = 2\mu/P. \tag{4.9}$$

Similar to Gorji, 2014, one can show that it is sufficient to solve a system of nine equations with c_{ij} and γ_i being unknowns to fulfill relaxation rates of monatomic gas which leads to a correct Prandtl number, i.e. $Pr = 2/3$;

$$\begin{aligned} &c_{ik}\langle M_k'M_j'\rangle + c_{jk}\langle M_k'M_i'\rangle \\ &+ \gamma_i\langle M_j'M_k'M_k'\rangle + \gamma_j\langle M_i'M_k'M_k'\rangle = 0 \end{aligned} \tag{4.10}$$

and

$$\begin{aligned} &c_{ik}\langle M_k'M_j'M_j'\rangle + 2c_{jk}\langle M_k'M_j'M_i'\rangle \\ &+ \gamma_i\Big(\langle M_j'M_j'M_k'M_k'\rangle - \langle M_j'M_j'\rangle\langle M_k'M_k'\rangle\Big) \\ &+ 2\gamma_j\Big(\langle M_j'M_i'M_k'M_k'\rangle - \langle M_j'M_i'\rangle\langle M_k'M_k'\rangle\Big) = \frac{5}{3\tau}\langle M_i'M_j'M_j'\rangle. \end{aligned} \tag{4.11}$$

Similar to DSMC, here we employ a particle Monte-Carlo scheme as samples of SDEs eq. (4.1). Therefore, we use the numerical solution of eq. (4.1) similar to what is suggested in Gorji and Jenny, 2014 with following explicit scheme

$$M_i^{n+1} = U_i + \alpha_{cell}\Big(M_i'^n e^{-\Delta t/\tau} + c_{ik}M_k'^n + \gamma_i(M_k'^n M_k'^n - 3kT/m) + \sqrt{\frac{2kT}{\tau m}}\xi_i\Big), \tag{4.12}$$

$$X_i^{n+1} = X_i^n + M_i^n\Delta t \tag{4.13}$$

where ξ_i is a normally distributed random variable and α_{cell} makes sure that kinetic energy in each cell is conserved

$$\alpha_{cell} = \frac{\langle M_k'^n M_k'^n\rangle}{\langle M_k'^{n+1} M_k'^{n+1}\rangle}. \tag{4.14}$$

Please note that summations in eq. (4.14) are only over particles within the cell. The outline of the quadratic Fokker-Planck model of ideal gas (IFP) is given in table 4.1.

4.4 Noise reduction

Since in the resulting numerical approximation of eq. (4.12) we employ finite number of computational particles, the mean and variance of $\boldsymbol{\xi}$ may deviate from the

1.	Stream particles according to eq. (4.13).
2.	Apply boundary conditions.
3.	Calculate moments of velocity in each cell.
4.	Calculate c_{ij} and γ_i from eqs. (4.10) and (4.11).
5.	Update velocity according to FP model eq. (4.12).
6.	Sample data.

TABLE 4.1: Outline of the IFP algorithm for each time step.

exact values. Gorji and Jenny, 2014 suggested a modification to produce the employed random numbers such that we make sure the employed random numbers have zero mean and unity variance. For n_p particles in a cell they proposed using η_i^j instead of ξ_i^j where $j = 1, ..., n_p$, $i = 1, 2, 3$ and

$$\hat{\xi}_i^j = \xi_i^j - \frac{\sum_{j=1}^{n_p} \xi_i^j}{n_p}, \tag{4.15}$$

$$\eta_i^j = \frac{\sum_{j=1}^{n_p} \hat{\xi}_i^j}{\sqrt{(\sum_{j=1}^{n_p} \hat{\xi}_i^j \hat{\xi}_i^j)/n_p}}. \tag{4.16}$$

Note that similar modification of random numbers was employed in this study.

Chapter 5

A Fokker-Planck Model for Dense Gases

In this chapter we devise a novel Fokker-Planck model for description of dense gases consistent with the Enskog equation. First, new terms that capture dense gas corrections to the pressure tensor and the heat fluxes will be introduced. Then, a numerical scheme for practical simulation of dense gases will be proposed.

Before proceeding to the rigorous derivation of the dense FP model, let us provide a rough idea with regards to the contribution of dense gas effects in the model. Motivated by the position correction scheme discussed in CBA § 3.2, we consider

$$dX_i = (M_i + \hat{A}_i)dt, \tag{5.1}$$

where $\hat{\boldsymbol{A}}$ would be the correction to the dilute molecular velocity $\boldsymbol{M}$. So, the question becomes how we fix $\hat{\boldsymbol{A}}$ to represent what CBA or more accurately, the Enskog equation provides? This thesis is about introducing a consistent $\hat{\boldsymbol{A}}$. Having the velocity evolution similar to IFP

$$dM_i = A_i dt + DdW_k \tag{5.2}$$

and using Itô's lemma, one can show that evolution of the MDF becomes

$$\frac{\partial \mathcal{F}}{\partial t} + \frac{\partial (\mathcal{F} V_i)}{\partial x_i} = -\frac{\partial (\mathcal{F} A_i)}{\partial V_i} - \frac{\partial (\mathcal{F} \hat{A}_i)}{\partial x_i} + \frac{1}{2}\frac{\partial^2}{\partial V_i \partial V_j}(D^2 \mathcal{F}). \tag{5.3}$$

The drift A_i and the diffusion D coefficients are also affected by the dense effects. In the following sections, first necessary modifications to these coefficients are described. Then, we propose a model for $\hat{A}_i$ in the position update.

5.1 Correction in Velocity Evolution

As discussed in § 4.1, drift and diffusion coefficients are calculated by satisfying relaxation rates of the shear stress and the heat fluxes. Since these rates differ slightly for the Enskog equation from the Boltzmann operator, A_i and D must be corrected such that eqs. (2.42) and (2.43) are satisfied instead. Our approach is

similar to what has been done by Gorji, 2014 with the exception that moments of Boltzmann are also multiplied by Enskog's factor Y. One can show that, similar to IFP, relaxation rates of quadratic model in a homogeneous setup are

$$\frac{\partial \pi_{ij}}{\partial t} = \rho\langle A_i M'_j + A_j M'_i + D^2\delta_{ij}\rangle \quad \text{and} \tag{5.4}$$

$$\frac{\partial q_i}{\partial t} = \frac{1}{2}\rho\langle A_i M'_j M'_j + 2A_j M'_j M'_i\rangle. \tag{5.5}$$

By matching eqs. (2.42) and (2.43) with eqs. (5.4) and (5.5), one can show that final expressions for A_i and D are exactly the expressions for IFP eqs. (4.10) and (4.11) with the only difference in the time scale τ. Substituting $\tau = \tau^k / Y$ we get

$$\begin{aligned} &c_{ik}\langle M'_k M'_j\rangle + c_{jk}\langle M'_k M'_i\rangle \\ &+ \gamma_i\langle M'_j M'_k M'_k\rangle + \gamma_j\langle M'_i M'_k M'_k\rangle = 0, \end{aligned} \tag{5.6}$$

$$\begin{aligned} &c_{ik}\langle M'_k M'_j M'_j\rangle + 2c_{jk}\langle M'_k M'_j M'_i\rangle \\ &+ \gamma_i\Big(\langle M'_j M'_j M'_k M'_k\rangle - \langle M'_j M'_j\rangle\langle M'_k M'_k\rangle\Big) \\ &+ 2\gamma_j\Big(\langle M'_j M'_i M'_k M'_k\rangle - \langle M'_j M'_i\rangle\langle M'_k M'_k\rangle\Big) = \frac{5Y}{3\tau^k}\langle M'_i M'_j M'_j\rangle \end{aligned} \tag{5.7}$$

and

$$\tau^k = \frac{2\mu^k}{P}. \tag{5.8}$$

Thus in each cell, the velocity of a particle evolves satisfying the relaxation rate conditions, i.e. eqs. (2.42) and (2.43), such that Prandtl number of 2/3 for the dilute monatomic gas limit can be obtained.

5.2 Correction in Position Evolution

As discussed in the beginning of this chapter, CBA gave us the suggestion that an extra advection is needed due to dense effects. Consequently, $\hat{A}_i$ was introduced to capture that effect. In this section, first the ansatz for $\hat{A}_i$ is given to obtain the total pressure and then it will be modified to obtain the correct heat conduction as well.

5.2.1 Total Pressure Tensor

In this section it will be shown that in order to get the correct pressure tensor, consistent with the Enskog equation i.e. eq. (2.46), $\hat{A}_i$ can be set to

$$\hat{A}_i = \alpha_{ij} v'_j. \tag{5.9}$$

First, let us make sure that the continuity is not touched. By integrating eq. (5.3) over the velocity space and using the fact that MDF and its derivative approach zero at the boundaries, we get

$$\frac{\partial \rho}{\partial t} + \frac{\partial(\rho U_i)}{\partial x_i} = -\frac{\partial}{\partial x_i}\Big(\rho \alpha_{ij} \langle M'_j \rangle\Big). \tag{5.10}$$

Note that by definition $\langle M'_j \rangle = 0$ and thus the right hand side of eq. (5.10) equals zero. In order to get to the momentum equation, we need to take the first velocity moment of eq. (5.3), meaning multiply both sides by V_k and take integral over the velocity space, i.e.

$$\frac{\partial(\rho U_k)}{\partial t} + \frac{\partial(\rho \langle M_i M_k \rangle)}{\partial x_i} = -\frac{\partial}{\partial x_i}(\rho \langle \hat{A}_i M_k \rangle). \tag{5.11}$$

By decomposing the velocity to its mean and fluctuation $\boldsymbol{V} = \boldsymbol{V}' + \boldsymbol{U}$, it follows

$$\frac{\partial(\rho U_k)}{\partial t} + \frac{\partial(\rho U_i U_k)}{\partial x_i} + \frac{\partial(\rho \langle M'_i M'_k \rangle)}{\partial x_i} + \frac{\partial}{\partial x_i}(\rho \langle \hat{A}_i M_k \rangle) = 0, \tag{5.12}$$

where $p^k_{ik} = \rho \langle M'_i M'_k \rangle$ is the kinetic pressure tensor. From definition of the pressure tensor in the kinetic theory we know that its trace would give us the equilibrium pressure and its deviatoric part gives the shear stress, i.e. eq. (2.10). However the pressure tensor of the dense gas is more complicated. As mentioned in § 2.3.1, the pressure tensor includes corrections due to the bulk viscosity, i.e. eq. (2.46). This means that we would need to incorporate for that in both trace and deviatoric part. Yet for simplicity, we assume that terms in $O(\epsilon^2)$ where $\epsilon = nb$ are negligible. By this assumption the terms including the divergence of the velocity drop out and the pressure tensor approximation arising from the Enskog equation becomes

$$\pi_{ij} = nkT(1 + nbY)\delta_{ij} + \rho(1 + 2nbY/5)\langle M'_{\langle i} M'_{j \rangle} \rangle. \tag{5.13}$$

Now as desired, the trace of π_{ij} gives us the equilibrium pressure and the deviatoric part gives the shear stress. Let us define the total equilibrium pressure and the total viscosity as following

$$p^{total}/p^k = 1 + nbY \quad \text{and} \tag{5.14}$$

$$\mu^{total}/\mu^k = 1 + 2nbY/5. \tag{5.15}$$

Again, p^k is the equilibrium pressure of the ideal gas, i.e. $p^k = nkT$. Thus it follows

$$p^{total}_{ik} = \frac{\mu^{total}}{\mu^k} \langle M'_{\langle i} M'_{k \rangle} \rangle + \frac{p^{total}}{p^k} \langle M'_j M'_j \rangle \delta_{ik}/3. \tag{5.16}$$

Therefore, the total pressure tensor of eq. (5.12) should be equal to

$$\langle M_i' M_k' \rangle + \langle \hat{A}_i M_k \rangle = \frac{\mu^{total}}{\mu^k} \langle M_{\langle i}' M_{k\rangle}' \rangle + \frac{p^{total}}{p^k} \langle M_j' M_j' \rangle \delta_{ik}/3. \tag{5.17}$$

Substituting our initial model for $\hat{A}_i$ eq. (5.9), one can show that the tensor coefficients α_{ij} must satisfy

$$\alpha_{ij} \langle M_j' M_k' \rangle = (\frac{\mu^{total}}{\mu^k} - 1) \langle M_{\langle i}' M_{k\rangle}' \rangle + (\frac{p^{total}}{p^k} - 1) \langle M_j' M_j' \rangle \delta_{ik}/3. \tag{5.18}$$

Up to this point the pressure tensor is corrected with the initial ansatz, eq. (5.9). By calculating α_{ij} coefficients such that eq. (5.18) is satisfied, one can obtain the total pressure tensor including dense effects. In the following section another term will be added to this model in order to obtain the total heat fluxes consistent with the Enskog equation.

5.2.2 Correcting Heat Fluxes

Taking the second velocity moment of eq. (5.3) and using our first ansatz for $\hat{A}_i$, eq. (5.9), one can easily note that we end up with more equations than the number of unknowns. To fix this, our ansatz for $\hat{A}_i$ is modified by adding another term, i.e.

$$\hat{A}_i = \alpha_{ij} v_j' + \beta_i (v_j' v_j' - 3kT/m). \tag{5.19}$$

In this study, we refer to this model as Quadratic Fokker Planck for Dense gases (Q-DFP). Similar to what we did for the momentum, first we show that the continuity is satisfied. Then, similar to what was done in § 5.2.1, an expression for α_{ij} and β_i can be derived to obtain the total pressure tensor including dense effects. Having done these, we take the second moment of eq. (5.3) and will obtain three more constraints on the unknown coefficients. The zeroth velocity moment of eq. (5.3) gives conservation of mass as expected

$$\frac{\partial \rho}{\partial t} + \frac{\partial (\rho U_i)}{\partial x_i} = -\frac{\partial}{\partial x_i} \Big(\rho \alpha_{ij} \langle M_j' \rangle \Big) - \frac{\partial}{\partial x_i} \Big(\beta_i (\langle M_j' M_j' \rangle - 3kT/m) \Big) = 0. \tag{5.20}$$

For the momentum equation, it is enough to substitute the modified ansatz for $\hat{A}_i$, eq. (5.19), in eq. (5.17)

$$\alpha_{ij} \langle M_j' M_k' \rangle + \beta_i \langle M_j' M_j' M_k' \rangle = \Big(\frac{\mu^{total}}{\mu^k} - 1 \Big) \langle M_{\langle i}' M_{k\rangle}' \rangle + \Big(\frac{p^{total}}{p^k} - 1 \Big) \langle M_j' M_j' \rangle \delta_{ik}/3. \tag{5.21}$$

Note that similar to what has been done in § 5.2.1, again we ignored $O(\epsilon^2)$ with $\epsilon = nb$. Therefore, μ^{total} and p^{total} are the expressions given in eqs. (5.14) and (5.15).

By taking the second velocity moment $\psi = V_k V_k/2$ of eq. (5.3), we can obtain the conservation of energy

$$\frac{1}{2}\frac{\partial}{\partial t}(\rho\langle M_k M_k\rangle) + \frac{1}{2}\frac{\partial}{\partial x_i}(\rho\langle M_i M_k M_k\rangle) = -\frac{1}{2}\frac{\partial}{\partial x_i}(\rho\langle \hat{A}_i M_k M_k\rangle). \tag{5.22}$$

Note the following expansions

$$\begin{aligned}\langle M_k M_k\rangle &= \langle (M'_k + U_k)(M'_k + U_k)\rangle = \langle M'_k M'_k\rangle + U_k U_k \\ &= \frac{3kT}{m} + U_k U_k\end{aligned} \tag{5.23}$$

and

$$\begin{aligned}\langle M_i M_k M_k\rangle &= \langle (M'_i + U_i)(M'_k + U_k)(M'_k + U_k)\rangle \\ &= \langle (M'_i + U_i)(M'_k M'_k + 2M'_k U_k + U_k U_k)\rangle \\ &= \langle M'_i M'_k M'_k + 2M'_i M'_k U_k + M'_i U_k U_k + U_i M'_k M'_k + 2U_i M'_k U_k + U_i U_k U_k)\rangle \\ &= \langle M'_i M'_k M'_k\rangle + 2\langle M'_i M'_k\rangle U_k + U_i\langle M'_k M'_k\rangle + U_i U_k U_k,\end{aligned} \tag{5.24}$$

are employed. Substituting these expansions back into eq. (5.22) one can show

$$\begin{aligned}&\frac{\partial}{\partial t}(\frac{3k}{2m}T + \frac{1}{2}\rho U_k U_k) + \frac{\partial}{\partial x_i}\Big(\frac{\rho}{2}\langle M'_i M'_k M'_k\rangle + \rho\langle M'_i M'_k\rangle U_k + \frac{3kT}{2m}U_i + \frac{1}{2}\rho U_i U_k U_k\Big) \\ &\qquad = -\frac{1}{2}\frac{\partial}{\partial x_i}\Big(\rho\langle \hat{A}_i M_k M_k\rangle\Big).\end{aligned} \tag{5.25}$$

As explained in chapter 2, the heat capacity at constant volume of a monatomic gas is $c_v = 3k/(2m)$. Also, the total energy of gas is defined as $E = c_v T + \rho U_i U_i/2$ where by using eq. (2.7) and eq. (2.12) we get

$$\frac{\partial E}{\partial t} + \frac{\partial}{\partial x_i}(q_i + \pi_{ik}U_k + U_i E) = -\frac{1}{2}\frac{\partial}{\partial x_i}(\rho\langle \hat{A}_i M_k M_k\rangle). \tag{5.26}$$

Let us substitute our quadratic model eq. (5.19) in the last term of eq. (5.26)

$$\langle \hat{A}_i M_k M_k\rangle = \alpha_{ij}\langle M'_j M_k M_k\rangle + \beta_i\Big(\langle M'_j M'_j M_k M_k\rangle - \frac{3kT}{m}\langle M_k M_k\rangle\Big). \tag{5.27}$$

Furthermore, by employing following expansions

$$\begin{aligned}\langle M'_j M_k M_k\rangle &= \langle M'_j(M'_k M'_k + 2M'_k U_k + U_k U_k)\rangle \\ &= \langle M'_j M'_k M'_k\rangle + 2U_k\langle M'_j M'_k\rangle \\ &= 2q_j/\rho + 2U_k\pi_{kj}/\rho\end{aligned} \tag{5.28}$$

and

$$\begin{aligned}\langle M_j' M_j' M_k M_k\rangle &= \langle M_j' M_j' (M_k' M_k' + 2M_k' U_k + U_k U_k)\rangle \\ &= \langle M_j' M_j' M_k' M_k'\rangle + 2U_k \langle M_j' M_j' M_k'\rangle + U_k U_k \langle M_j' M_j'\rangle \\ &= \langle M_j' M_j' M_k' M_k'\rangle + 4U_k q_k/\rho + U_k U_k \frac{3kT}{m}, \end{aligned} \tag{5.29}$$

we get

$$\begin{aligned}\frac{\partial E}{\partial t} + \frac{\partial}{\partial x_i}(q_i + \pi_{ik}U_k + U_i E) + \frac{\partial}{\partial x_i}\Big(&\alpha_{ij} q_j + \alpha_{ij} U_k \pi_{kj} + \beta_i \frac{\rho}{2}\langle M_j' M_j' M_k' M_k'\rangle \\ &+ 2\beta_i U_k q_k + \beta_i \frac{\rho}{2}\frac{3kT}{m} U_k U_k - \frac{\rho\beta_i}{2}\Big(\frac{3kT}{m}\Big)^2 \\ &- \beta_i \frac{\rho}{2}\frac{3kT}{m} U_k U_k\Big) = 0. \end{aligned} \tag{5.30}$$

Considering the relation found from the momentum equation eq. (5.21), we get

$$\begin{aligned}&\frac{\partial E}{\partial t} + \frac{\partial}{\partial x_i}[U_k(\frac{\mu^{total}}{\mu^k}\pi_{\langle ik\rangle} + \frac{p^{total}}{p^k}\pi_{jj}\delta_{ik}/3)] + \frac{\partial}{\partial x_i}(U_i E) \\ &\quad + \frac{\partial}{\partial x_i}\Big(q_i + \alpha_{ij} q_j + \beta_i \frac{\rho}{2}\langle M_j' M_j' M_k' M_k'\rangle - \frac{\rho\beta_i}{2}\Big(\frac{3kT}{m}\Big)^2\Big) = 0. \end{aligned} \tag{5.31}$$

Here is the place to set the heat fluxes to what we want it to become. As mentioned in § 5.2.1, we ignore $O(\epsilon^2)$ with $\epsilon = nb$. This assumption also simplifies the total heat flux eq. (2.47) and thus we get

$$q_i = (1 + 3nbY/5)\langle M_i' M_j' M_j'\rangle. \tag{5.32}$$

This implies the total heat conductivity κ^{total}

$$\kappa^{total}/\kappa^k = 1 + 3nbY/5 \tag{5.33}$$

including dense effects. Therefore, we want the heat fluxes of eq. (5.31) satisfy

$$q_i + \alpha_{ij} q_j + \beta_i \frac{\rho}{2}\langle M_j' M_j' M_k' M_k'\rangle - \frac{\rho\beta_i}{2}\Big(\frac{3kT}{m}\Big)^2 = \frac{\kappa^{total}}{\kappa^k} q_i. \tag{5.34}$$

Taking q_i to the right hand side we get

$$\alpha_{ij} q_j + \beta_i \frac{\rho}{2}\langle M_j' M_j' M_k' M_k'\rangle - \frac{\rho\beta_i}{2}\Big(\frac{3kT}{m}\Big)^2 = (\frac{\kappa^{total}}{\kappa^k} - 1) q_i, \tag{5.35}$$

or

$$\alpha_{ij}\langle M'_j M'_k M'_k\rangle + \beta_i\langle M'_j M'_j M'_k M'_k\rangle - \beta_i\Big(\frac{3kT}{m}\Big)^2 = (\frac{\kappa^{total}}{\kappa^k} - 1)\langle M'_i M'_k M'_k\rangle. \quad (5.36)$$

Thus, eq. (5.36) gives another constraint on our model to make sure that the total heat fluxes can be achieved by using the quadratic model, i.e. eq. (5.19), for the Fokker-Planck description of dense gases.

5.2.3 Summary of the Proposed Model

As discussed in previous sections, the effects of molecular diameter can be included in the position evolution of particles. As it has been justified, the Q-DFP ansatz

$$\hat{A}_i = \alpha_{ij}v'_j + \beta_i(v'_j v'_j - 3kT/m) \quad (5.37)$$

leads to correct viscosity and heat conductivity based on the Enskog equation; as long as $O((nb)^k)$ terms with $k > 1$ are neglected. Furthermore, we will refer to the case of $\boldsymbol{\beta} = 0$ as the Linear Dense FP model (L-DFP). Note that L-DFP only accounts for correct viscosities while Q-DFP provides a more complete model by giving correct heat conductivities as well.

Putting everything together and using Ito's lemma, we get the following set of SDEs

$$dM_i = \Big(-\frac{Y}{\tau}M'_i + c_{ij}M'_j + \gamma_i(M'_j M'_j - \frac{3kT}{m})\Big)dt + \sqrt{\frac{2kTY}{\tau m}}dW_k \quad \text{and} \quad (5.38)$$

$$dX_i = M_i dt + \Big(\alpha_{ij}M'_j + \beta_i(M'_j M'_j - 3kT/m)\Big)dt. \quad (5.39)$$

The coefficients c_{ij} and γ_i are calculated based on the relaxation rates with expressions given in eqs. (5.6) and (5.7), as explained in § 5.1. Effects of the diameter are captured by α_{ij} and β_i from eqs. (5.21) and (5.36) which forms a system of 12 equations for each cell.

5.3 Numerical Scheme

Since the velocity update is quite similar to the IFP model, the only change is due to the time scale τ^{total} according to eq. (5.8). Hence, we only need to add the extra advection to the position update resulting in

$$M_i^{n+1} = U_i^n + \alpha_{cell}\Big(M_i'^n e^{-\Delta tY/\tau} + c_{ik}M_k'^n + \gamma_i(M_k'^n M_k'^n - 3kT/m) + \sqrt{\frac{2kTY}{\tau m}}\xi_i\Big) \quad (5.40)$$

and

$$X_i^{n+1} = X_i^n + M_i^n\Delta t + \Big(\alpha_{ij}M_j'^n + \gamma_i(M_j'^n M_j'^n - 3kT/m)\Big)\Delta t. \quad (5.41)$$

1.	Calculate moments of the velocity in each cell.
2.	Calculate α_{ij} and β_i from eqs. (5.6) and (5.7).
3.	Stream particles using eq. (5.41).
4.	Apply boundary conditions.
5.	Calculate moments of the velocity in each cell.
6.	Calculate c_{ij} and γ_i from eqs. (4.10) and (4.11).
7.	Update the velocity according to FP model eq. (5.40).
8.	Sample data.

TABLE 5.1: Outline of Q-DFP for dense gases at each time step.

In eq. (5.41), we assumed that the velocity does not change in Δt which is a simplification to avoid the complexity with regards to the integration. One might try to get an exact position update from the velocity profile by taking integral over the time step

$$X_i^{n+1} = X_i^n + \int_t^{t+\Delta t} \Big(M_i + \alpha_{ij} M_j' + \gamma_i (M_j' M_j' - 3kT/m)\Big) dt. \tag{5.42}$$

Nevertheless, in this study we stick to eq. (5.41) and admit the integration error. An outline of the Q-DFP model of dense gas flows is given in table 5.1.

Chapter 6

Simulation Studies

In this chapter, the simulation results of several simple test cases are reported. These examples are meant to show the accuracy of Q-DFP model. For comparison, results from DSMC, CBA and IFP model are also calculated. Since directly solving the Enskog equation is quite challenging and expensive, comparisons were made with respect to the CBA results for the transport coefficients at moderate densities, i.e. $n\sigma^3 < 0.4$. CBA is used since according to Alexander et al., 1995 it predicts relatively similar results compared with the Enskog and MD solutions.

Argon with properties mentioned in table 6.1 is used for all the simulations. The molecular values are taken from Bird, 1994. μ is the viscosity of dilute Argon and ω is the exponent factor in scaling viscosity with respect to the temperature i.e. $\mu/\mu_0 = (T/T_0)^{\omega}$. Note that $\omega = 1/2$ for HS molecular model. σ indicates diameter and m is molecular mass.

$\mu\ [kg.m^{-1}.s^{-1}]$	$\omega\ [-]$	$\sigma\ [m]$	$m\ [kg]$	$\kappa\ [W.m^{-1}.K^{-1}]$
2.117×10^{-5}	0.5	3.628×10^{-10}	6.633×10^{-26}	0.01625

Table 6.1: Properties of Argon.

Iso-thermal walls are considered in all the simulations, i.e. the temperature of surface is kept constant at T_w. The boundary conditions are set such that velocity represents the equilibrium state for such a temperature. For instance, velocity of particles hitting a wall with normal in x_2 direction and driven with velocity U_w in x_1 direction are as the following

$$M_1 = \sqrt{\frac{k_b T_w}{m}}\mathcal{N}(0,1) \pm U_w, \tag{6.1}$$

$$M_2 = \pm\sqrt{\frac{2k_b T_w}{m}}\sqrt{-ln\Big(\mathcal{R}(0,1)\Big)}, \tag{6.2}$$

$$M_3 = \sqrt{\frac{k_b T_w}{m}}\mathcal{N}(0,1), \tag{6.3}$$

where $\mathcal{N}(0,1)$ is a normal random number with zero mean and standard deviation of one. $\mathcal{R}(0,1)$ stands for a random number with the uniform distribution between zero and one. Position of particles hitting the walls are updated using the new velocity and the remainder portion of the time step. For details on thermal walls, reader is referred to Bird, 1994. Also, note that in all of the simulations, except for

TABLE 6.2: Performance and memory of Intel(R) Xeon(R) CPU X7542.

Max Turbo Frequency	2.8 GHz
L2 cache	256 K
L3 cache	18 MB

performance reports, dimensions are picked such that Knudsen number $Kn = 0.01$ is obtained.

In all simulations of CBA and DSMC, small enough time step is chosen

$$\Delta t = 0.01 \frac{min(\lambda, L/n_c)}{max(U_w, U_{th})}, \tag{6.4}$$

where U_{th} is the thermal velocity of the wall i.e. $U_{th} = \sqrt{kT_w/m}$ and λ the mean free path. Here, n_c indicates the number of cells in each direction. In case of the Fokker-Planck based simulations, CFL condition as suggested by Gorji and Jenny, 2015 is used for determining the time step size, i.e.

$$\Delta t \leq \frac{1}{2} \frac{L/n_c}{max(U_w, U_{th})}. \tag{6.5}$$

In all the simulation studies, the box geometry is adopted. Walls are kept at the constant temperature while they can move by a given velocity U_w. Figure 6.1 shows the corresponding schematic.

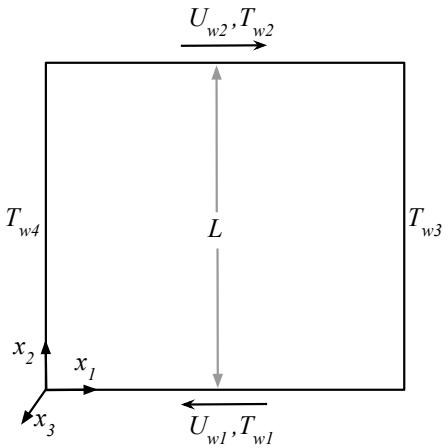

FIGURE 6.1: Schematic of the simulation setup.

In all simulations, single core with one thread of Intel(R) Xeon(R) CPU X7542 with specification given in table 6.2 was utilized for the computations.

6.1 Equilibrium Box

In order to check whether the proposed DFP give us the equilibrium pressure consistent with the Enskog solution, equilibrium conditions are imposed on the gas. Particles are uniformly distribution in a box where velocities are set based on the

Maxwellian distribution. The iso-thermal stationary walls at $T_w = 273\ K$ are considered. Therefore, the gas is at rest with no external force or a temperature gradient. Thus, the macroscopic quantities of the gas do not change in time and the MDF remains Maxwellian.

The pressure is calculated based on its fundamental definition i.e. force per area that wall experience from the gas particles. This force is nothing but the rate of change of the momentum of these particles. Therefore, the pressure is calculated from

$$P = \frac{1}{At^f}\Big(\sum_{t=0}^{t^f}\sum_{j=1}^{N_c}\Delta(mM_j)\Big). \tag{6.6}$$

Here A is the total area of faces of the box. In case of a cubic box it will be $A = 6L^2$. t^f is the final time when sampling terminates. N_c indicates the number of particles that hit the wall during each time step.

10^4 particles are employed in a cell which is left at rest. Figure 6.2 indicates accuracy of the proposed dense FP models compared to CBA, DSMC and IFP. It is interesting to see that Q-DFP and L-DFP models give better agreement compared to CBA, where the latter over-predicts the value $nk_bT(1 + nbY)$.

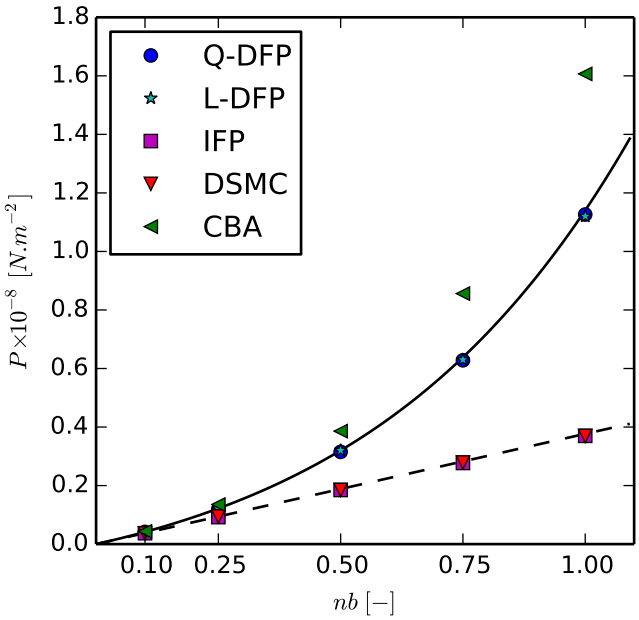

FIGURE 6.2: Equilibrium pressure of gas at $Kn = 0.01$ obtained from L-DFP, Q-DFP, IFP, DSMC and CBA. Solid black line indicates $P = nk_bT(1 + nbY)$ and dashed line is $P = nk_bT$.

As discussed in § 3.2, CBA becomes extremely costly as the gas becomes denser. Achieving a better performance was one of the main motivations behind developing a dense FP model. As a rough cost comparison, a box at $Kn = 0.01$ and a gas at $nb = 0.1$ are chosen while the density is increased without changing the dimensions. The cost of proposed FP models have no correlation with the density of the gas, as expected. However, CBA becomes expensive as the gas becomes

denser. Like DSMC, the number of collision candidates in CBA is a function of the density, i.e. quadratic correlation. One can see the mentioned reasoning clearly in Figure 6.3. Note that the CPU times include both streaming and velocity update.

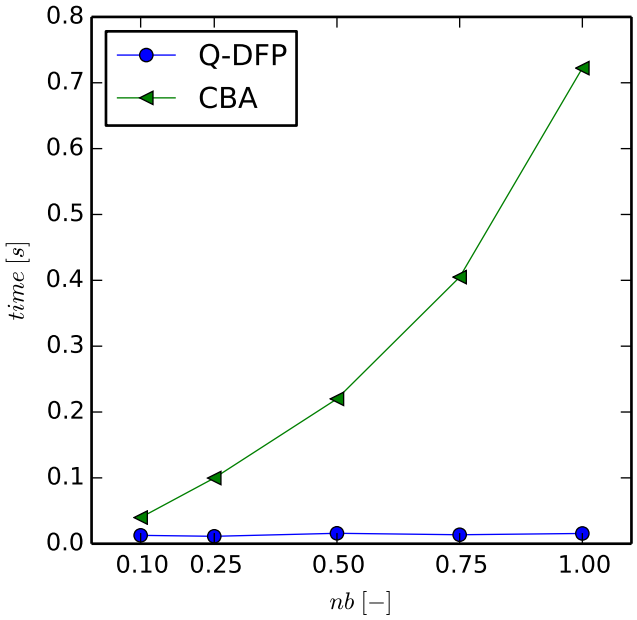

FIGURE 6.3: Execution time of Q-DFP and CBA for same amount of simulation time.

6.2 Couette Flow

In order to assess the shear viscosity of the gas, the planar Couette flow is considered here. The idea is that by moving walls in opposite directions, a gradient of the bulk velocity can be obtained such that the viscosity can be calculated from its relation with the shear stress. Here, relations obtained from the Chapman-Enskog expansion come to our help in measuring viscosity at low Knudsen flow. As explained in §§ 2.2.2 and 2.3.2, one can relate the pressure tensor and the heat fluxes to the gradients of the bulk velocity and the temperature, i.e. eqs. (2.30), (2.31), (2.50) and (2.51).

Let the walls of a box be large enough in x_1 and x_3 dimensions. Thus, one can assume that the gas behavior is one dimensional in x_2 dimension. By moving walls with normal in x_2 by $U_w = (\pm 300, 0, 0)^T$ $[m/s]$ in opposite directions, the desired shear stress can be produced. Ignoring derivatives with respect to x_1 and x_3, and knowing that divergence of the bulk velocity is very small, $\partial U_k/\partial x_k \to 0$, one can show that the pressure tensor for ideal and dense gases are

$$p_{12}^{ideal} = -\mu^k \frac{\partial U_1}{\partial x_2} \quad and \tag{6.7}$$

$$p_{12}^{dense} = -\Big(\frac{\mu^k}{Y}(1 + 2nbY/5)^2\Big)\frac{\partial U_1}{\partial x_2}, \tag{6.8}$$

respectively. The dilute gas regime should give us $\mu^{ideal} = \mu^k$ while the dense one gives $\mu^{dense} = \mu^k(1 + 2nbY/5)^2/Y$. Gradient of the bulk velocity was calculated using a simple second order central difference discretization upon the averaged velocity of each cell. Furthermore, sampling the pressure tensor can be obtained according to

$$\begin{aligned} p_{12} &= \rho\langle M_1' M_2' \rangle = \rho\langle (M_1 - U_1)(M_2 - U_2) \rangle \\ &= \rho\Big(\langle M_1 M_2 \rangle - U_1 U_2\Big). \end{aligned} \tag{6.9}$$

Therefore, we can do time averaging in order to estimate U_1, U_2 and $\langle M_1 M_2 \rangle$. Also, note that the viscosity scales with the temperature. Therefore, in order to compare the calculated viscosities at the reference temperature $T_{ref} = 273\ K$, $\mu(T)$ has to be scaled back to the reference value.

Convergence studies on the spatial refinement lead us to 200 computational cells in x_2. Besides, 1000 particle per cell were employed. Dimensions are set to reach $Kn = 0.01$ and $nb = 0.4$.

Figure 6.4 depicts the scaled viscosity back into the reference temperature. For the reference, exact values are also plotted, i.e. $\mu_{ref}^{ideal} = 2.117 \times 10^{-5} kg\ m^{-1} s^{-1}$ as in black dashed line and $\mu_{ref}^{dense} = \mu_{ref}^{ideal}(1 + 2nbY/5)^2/Y$ as black solid line. As expected, IFP and DSMC predict μ_{ref}^{ideal} with a decent accuracy. However, similar to what Alexander et al., 1995 have reported, CBA over predicts viscosity μ_{ref}^{dense}. The proposed L-DFP and Q-DFP both provide a good agreement against the exact values.

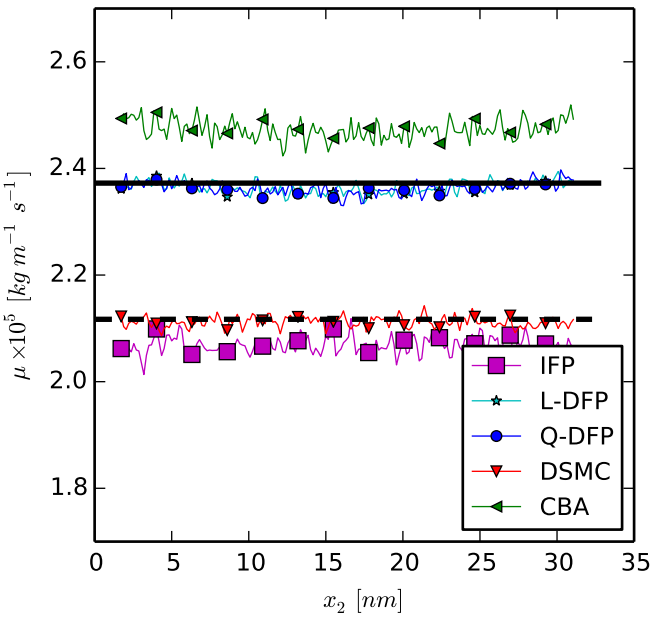

FIGURE 6.4: Calculated viscosity from the Couette flow simulations with $Kn = 0.01$ and $nb = 0.4$ using Q-DFP, IFP, DSMC and CBA. Solid line indicates $\mu_{ref}^{dense} = \mu_{ref}^{ideal}(1 + 2nbY/5)^2/Y$ and dashed line μ_{ref}^{ideal}.

The shear stress and the velocity profile of the Couette flow simulations are shown in Figure 6.5. Velocities are almost identical while one can see differences in the

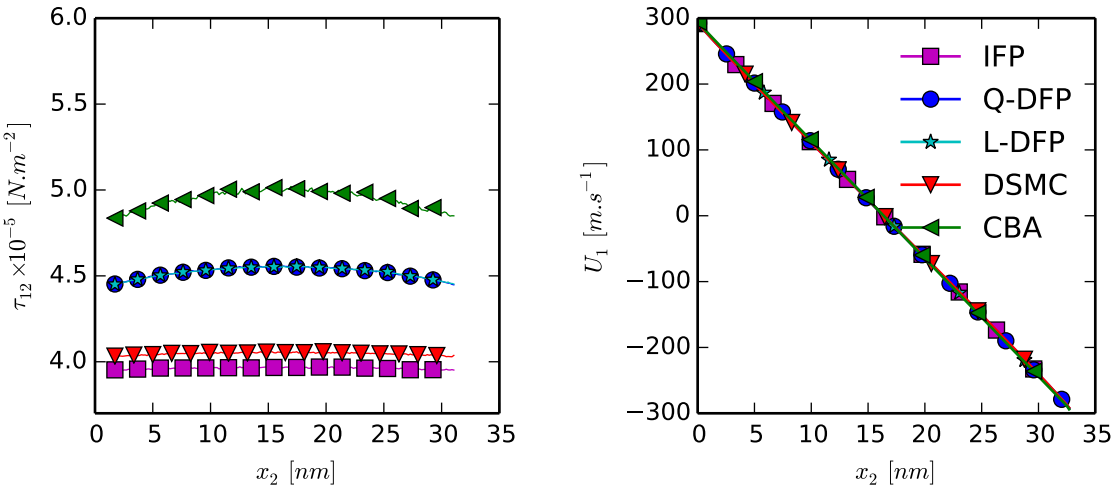

FIGURE 6.5: The shear stress and velocity profiles of the Couette flow obtained from Q-DFP, IFP, DSMC and CBA where $Kn = 0.01$ and $nb = 0.4$.

shear stress. It is not a surprise that CBA gives a higher shear stress than our proposed dense FP models.

6.3 Fourier Flow

In this section, the heat conduction will be evaluated in the dense regime. As explained in § 5.2.2, the quadratic model is proposed to impose the dense effect on the heat conduction of gas. Here, by imposing a temperature gradient in our box, we can easily get the thermal conductivity of the gas from Fourier's law. The setup is similar to the one of the Couette flow § 6.2, except for boundary conditions. Similar to the Couette case, one can again expect to see an one dimensional flow profile which is driven due to the temperature difference of the walls. Fourier's law together with the Chapman-Enskog heat conductivity values give us

$$q_2^{ideal} = -\kappa^k \frac{\partial T}{\partial x_2} \quad \text{and}$$
$$q_2^{dense} = -\Big(\frac{\kappa^k}{Y}(1 + 3nbY/5)^2\Big)\frac{\partial T}{\partial x_2}, \tag{6.10}$$

for dilute and dense gas, respectively. Therefore, the heat conductivity of dense gas reads $\kappa^{dense} = \kappa^k(1 + 3nbY/5)^2/Y$. One can evaluate this transport coefficient by calculating the heat flux q_2 and the temperature gradient $\partial T/\partial x_2$ from simulations. The temperature gradient is calculated using a central finite difference on the time averaged temperature profile. The heat fluxes are calculated based on

$$q_2 = \rho\langle M_2' M_j' M_j' \rangle = \rho\langle (M_2 - U_2)(M_j - U_j)(M_j - U_j)\rangle$$
$$= \rho\Big(\langle M_2 M_j M_j\rangle - 2\langle M_2 M_j\rangle U_j - \langle M_j M_j\rangle U_2 + 2\langle M_j\rangle U_j U_2\Big). \tag{6.11}$$

The temperature gradient is imposed by setting $T_{w1} = 300\ K$ and $T_{w2} = 900\ K$. Here we set the density such that $nb = 0.1$ and based on $Kn = 0.01$ the distance between the two walls is found. After convergence studies, we observed that 500 cells give a fine accuracy for capturing the temperature gradient. Also, note that 1000 particles per cell was employed in all the simulations.

Figure 6.6 shows the thermal conductivity calculated from the Fourier flow. The solid lines indicates exact values scaled to the number density and the temperature of dense gas, while the dashed lines account for the ideal gas. Thus, the following scalings are adopted

$$\kappa^{ideal}(T)/\kappa(T_{ref}) = (T/T_{ref})^{\omega} \quad \text{and} \tag{6.12}$$

$$\kappa^{dense}(T)/\kappa(T_{ref}) = (T/T_{ref})^{\omega}(1 + 3nbY/5)^2/Y. \tag{6.13}$$

As shown in Figure 6.6, as expected the IFP model gives the reference heat conductivity of the dilute gas. For such a moderate dense gas, as expected, CBA predicts the thermal conductivity close to the benchmark. Q-DFP also predicts κ^{dense} with a good accuracy. This validates our model for the heat conduction correction according to the Enskog equation.

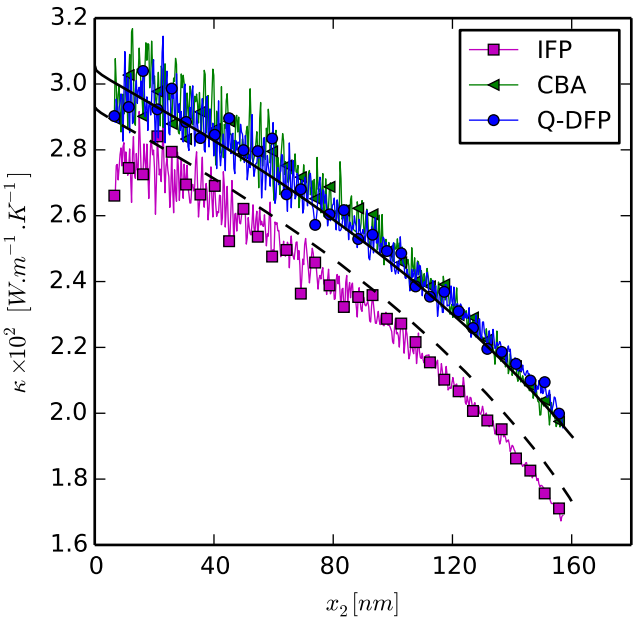

FIGURE 6.6: Heat conductivity calculated from Fourier flow with $Kn = 0.01$ and $nb = 0.1$ using proposed Q-DFP, IFP and CBA.

Moreover, the bulk temperature and the heat flux are plotted along x_2. Indeed both temperature and heat flux are very similar for CBA and Q-DFP. Note that this similarity is only the case for very moderate dense gases. As nb increases, again CBA ends up over-predicting heat flux and its heat conductivity diverges from DFP and the exact heat conductivity obtained from the Enskog equation.

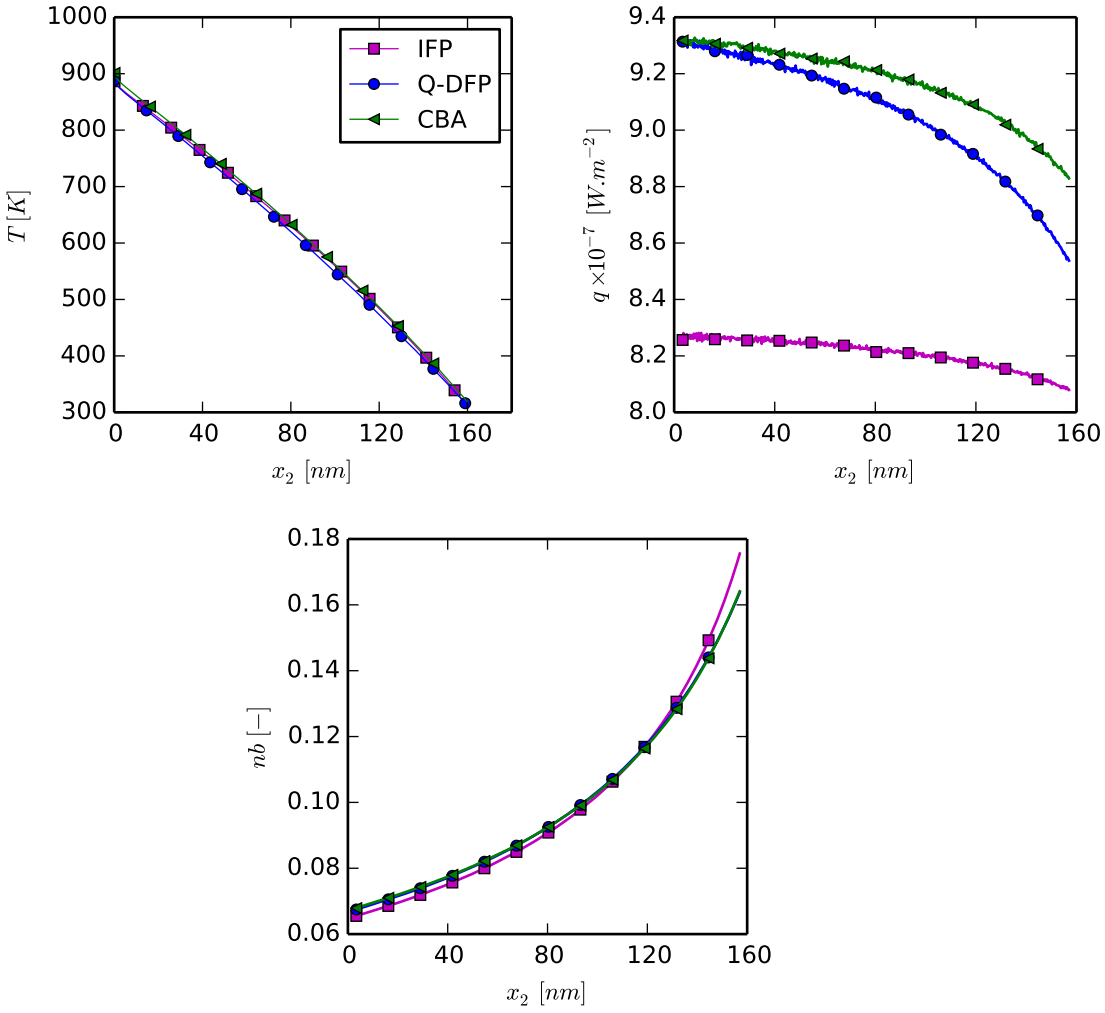

FIGURE 6.7: Temperature, heat flux and *nb* profiles of Fourier flow with $Kn = 0.01$ and initial $nb = 0.1$ calculated using Q-DFP, IFP and CBA.

Chapter 7

Conclusion and Outlooks

In this study, a Fokker-Planck description suitable for dense monatomic gas flows was developed. In comparison to the original model of Jenny et al., 2010; Gorji and Jenny, 2014, a drift-like term in evolution of the position is introduced. First a linear model for this velocity correction was proposed in order to incorporate the dense effects in the pressure tensor. To obtain correct heat fluxes a quadratic model was then added to the introduced term. Several examples were simulated such that accuracy of derivation could be evaluated. The equilibrium pressure was obtained by simulating a gas in an insulated box. Correction to the shear stress for both linear and quadratic models were tested by simulating the Couette flow. Then, the modified heat conductivity was measured by simulating the Fourier problem. By these examples, we can conclude that the derivation given in chapter 5 is consistent with the Enskog expansions in the give range of nb. Also, it was shown that numerical complexity of the Fokker-Planck model of dense gases, unlike CBA, has no correlation with the density.

There are several improvements that can be considered for future studies. A more accurate position update, i.e. eq. (5.42), could be implemented instead of a simple Euler method used here. Also, here we have used a quadratic model for the kinetic part, i.e. velocity update, which is sufficient for obtaining correct Prandtl number. However, for stability reasons, it is suggested to use a cubic model as explained by Gorji et al., 2011.

One of the assumptions that we made was ignoring terms in the order or higher than (ϵ^2) in the total pressure tensor and the heat fluxes, i.e. $\epsilon = nb$. This helped us with extracting the equilibrium pressure from the trace of pressure tensor and setting it to its corresponding equation of state for dense gases, i.e. eqs. (5.14) and (5.17). This implied ignoring the dense effects on the bulk viscosity of the gas. For future studies, it might be possible to include the bulk viscosity modification by adding a diffusive term in velocity update of the proposed dense Fokker-Planck model.

Moreover, in this study we considered only Hard Sphere (HS) as molecular model. Basically, the Enskog equation is designed for HS. Therefore, for more dense gases or liquids, it is worth mentioning the need for more accurate collision operators such that complicated potentials, e.g. the Lennard-Jones potential, could be modeled in the kinetic theory. That way, the kinetic theory can be further extended for accurate predictions of liquid flows as well.

Bibliography

Alexander, Francis J., Alejandro L. Garcia, and Berni J. Alder (1995). "A consistent Boltzmann algorithm". In: *Physical Review Letters* 74.26, pp. 5212–5215. DOI: 10.1103/PhysRevLett.74.5212.

Bird, G. a. (1963). "Approach to Translational Equilibrium in a Rigid Sphere Gas". In: *Physics of Fluids* 6.10, p. 1518. ISSN: 00319171. DOI: 10.1063/1.1710976. URL: http://scitation.aip.org/content/aip/journal/pof1/6/10/10.1063/1.1710976.

Bird, G. A. (1994). *Molecular Gas Dynamics and the Direct Simulation of Gas Flows*. Oxford University Press Inc.

Cercignani, Carlo (1988). *The Boltzmann Equation and its Applicatoins*. Vol. 67. Springer Verlag, New York. ISBN: 9781461269953.

Chapman, Sydney and T. G. Cowling (1953). *The Mathematical Theory of Non-Uniform Gases*.

Gardiner, Crispin W. (1996). *Handbook of stochastic methods: For Physics, Chemistry and the Natural Sciences*. Vol. 13, p. 422.

Gorji, M. Hossein and Patrick Jenny (2013). "A Fokker-Planck based kinetic model for diatomic rarefied gas flows". In: *Physics of Fluids* 25.6. ISSN: 10706631. DOI: 10.1063/1.4811399.

Gorji, M. Hossein and Patrick Jenny (2014). "An efficient particle Fokker-Planck algorithm for rarefied gas flows". In: *Journal of Computational Physics* 262, pp. 325–343. DOI: 10.1016/j.jcp.2013.12.046.

Gorji, M. Hossein and Patrick Jenny (2015). "Fokker-Planck-DSMC algorithm for simulations of rarefied gas flows". In: *Journal of Computational Physics* 287, pp. 110–129. DOI: 10.1016/j.jcp.2015.01.041.

Gorji, M.H., M. Torrilhon, and P. Jenny (2011). "Fokker-Planck model for computational studies of monatomic rarefied gas flows". In: *Journal of Fluid Mechanics* 680, pp. 574–601. DOI: 10.1017/jfm.2011.188.

Gorji, Mohammad Hossein (2014). "Fokker-Planck Solution Algorithm for Rarefied Gas Flows and Applications of Complex Gas-Surface Interactions". PhD thesis. Swiss Federal Institute of Technology in Zurich (ETHZ).

Hirschfelder, Joseph O., Charles F. Curtiss, and R. Byron Bird (1963). *The Molecular Theory of Gases and Liquids*.

Jenny, Patrick, Manuel Torrilhon, and Stefan Heinz (2010). "A solution algorithm for the fluid dynamic equations based on a stochastic model for molecular motion". In: *Journal of Computational Physics* 229.4, pp. 1077–1098. DOI: 10.1016/j.jcp.2009.10.008.

Truesdell, C. and R. G. Muncaster (1980). *Fundamentals of Maxwell's kinetic theory of a simple monatomic gas*, pp. 1–623. ISBN: 0127013504. DOI: 10.1016/S0079-8169(08)62263-1.

Ullo, J. J. and Sidney Yip (1984). "Molecular dynamics of dense gases: Effects of continuous potentials". In: *Phys. Rev. A* 29 (4), pp. 2092–2097. DOI: 10.1103/PhysRevA.29.2092. URL: http://link.aps.org/doi/10.1103/PhysRevA.29.2092.